

## Thermodynamics of H–T phase transition in MoS<sub>2</sub> single layer

I. S. Popov, A. N. Enyashin

Institute of Solid State Chemistry UB RAS, Ekaterinburg, Russia  
popov@ihim.uran.ru

PACS 64.70.Kb, 62.20.Fe, 61.72.Bb, 61.50.Ah

DOI 10.17586/2220-8054-2019-10-4-420-427

Molybdenum disulfide is a title compound among the layered metal dichalcogenides, being a prominent tribological agent and vital platform for catalysts. The properties of a MoS<sub>2</sub> layer can vary widely, depending upon polymorphic composition. Here, using the density-functional theory calculations, the potential energy surfaces for polymorphic H- and T-MoS<sub>2</sub> layers are mapped. While the energy barriers for H→T and T(T′)→H transitions are found to be in fair agreement with previous studies which employed the nudged elastic band method, the bird's-eye view at the energy landscape of MoS<sub>2</sub> layer has disclosed the as-yet undescribed energy plateau attributed to an intermediate – square lattice of MoS<sub>2</sub> layer (S-MoS<sub>2</sub>). The stability, structural and electronic properties of S-MoS<sub>2</sub> are discussed in comparison with those for H- and T-MoS<sub>2</sub> layers.

**Keywords:** layered chalcogenides, molybdenum sulfide, phase transition, DFT calculations.

*Received: 13 August 2019*

### 1. Introduction

Molybdenum disulfide MoS<sub>2</sub> yields a wealth of crystalline and nanostructured materials, well respected in numerous tribological applications [1] and promising in the fields of nanoelectronics [2, 3], photovoltaics [4] and photodetectors [5]. This compound under normal conditions crystallizes in the layered 2H<sub>b</sub>-MoS<sub>2</sub> phase, which hexagonal unit cell includes two anti-parallel layers held together by van der Waals' interactions [6]. The S atoms in every layer (henceforth, H-layer) are arranged in trigonal prisms with the bases forming two S atom planes, while the Mo atoms are located in the centers of these prisms. Related 3R-MoS<sub>2</sub> polytype, containing three parallel H-layers in the hexagonal unit cell, was also found in nature [7]. 2H<sub>b</sub>-MoS<sub>2</sub> modification is a semiconductor with an indirect intrinsic band gap ( $E_g$ ) equal to 1.2 eV [2]. The exfoliation of either 2H<sub>b</sub>-MoS<sub>2</sub> or 3R-MoS<sub>2</sub> crystals into individual monolayers leads to the rise of a direct intrinsic band gap of material  $E_g = 1.8$  eV [2].

Increasing of the pressure to ~20 GPa initiates emergence of another polytypic form – 2H<sub>a</sub>-MoS<sub>2</sub> [8, 9]. This phase differs from 2H<sub>b</sub>-MoS<sub>2</sub> by a shift of two H-layers relative to each other and a decrease in the interlayer distance. The compound 2H<sub>a</sub>-MoS<sub>2</sub> exhibits metallic properties [9].

A heavy doping of the MoS<sub>2</sub> lattice by electrons stimulates stabilization of another polymorph – the layered 1T-MoS<sub>2</sub> phase – regardless of the source of excessive electrons [10–14]. The S atoms in the single layer of 1T-MoS<sub>2</sub> (henceforth, T-layer) are arranged as octahedra with Mo atoms in the center. 1T-MoS<sub>2</sub> is characterized by the absence of the band gap [15]. This phase is of interest in the development of supercapacitors [16, 17] and memristors [18, 19]. Due to natural metal-like character the catalytic properties of 1T-MoS<sub>2</sub> in the hydrogen evolution reaction may be significantly stronger than those of semiconducting 2H<sub>b</sub>-MoS<sub>2</sub> [10, 20].

A spontaneous reconstruction of the ideal hexagonal 1T-MoS<sub>2</sub> monolayer results in several superstructures, collectively designated as the T' phase [21]. According to quantum-chemical calculations, 1T'-MoS<sub>2</sub> superstructures have a lower energy than the energy of hexagonal 1T-MoS<sub>2</sub> crystals, since a band gap  $E_g = 50$  meV is open in the band structure of the precursor 1T-MoS<sub>2</sub>, due to the spin-orbit coupling (SOC) at the Dirac cone [22]. The band gap opening due to SOC is of particular interest, as it is related to 2D topological insulators [22, 23].

A mixture of the H, T, and T' phases within single MoS<sub>2</sub> layer was observed in experiments on stabilization of the T-phase by intercalating alkali metals into the interlayer space, followed by exfoliation [24, 25]. Due to the vital potential of a metal-like MoS<sub>2</sub> for practical applications, the evaluation of its controlled fabrication is of greatest importance. Hence, a deep understanding of the phase transition from a stable 2H<sub>b</sub>-MoS<sub>2</sub> polymorph to a metastable 1T-MoS<sub>2</sub> polymorph is required. The mechanism of the H-T phase transition was suggested earlier, as the one involving the gliding of atomic S planes [22, 26–29]. The magnitude of the energy barrier for H→T and T(T′)→H transitions was estimated using the DFT calculations with the nudged elastic band (NEB) method as 1.5–1.9 and 0.7–1.0 eV, respectively. According to [27], the magnitude of the energy barrier can drop from 1.6 to 0.3 eV, when 4e<sup>−</sup> are injected per MoS<sub>2</sub> unit. The formation energy of 1T-MoS<sub>2</sub> gradually decreases from +0.8 eV in neutral state to −0.3 eV in such extremely charged 4e<sup>−</sup> state. The decrease of both the energy barrier and the formation energy of the T-phase by the charging have also been obtained using the DFT calculations [22]. Experimentally, the H→T phase transition was registered in Re-doped molybdenum disulfide using the method of scanning transmission electron microscopy [28].

The mechanism observed in [28] involves the gliding of atom planes of sulfur and/or molybdenum and requires an intermediate phase (so-called  $\alpha$ -phase) as a precursor. A seed of the T-phase originates from the appearance of two  $\alpha$ -phase bands that are located relative to each other at an angle of 60°.

Structural phase transition can significantly alter the properties of solids without modifying their chemical composition. Understanding the mechanisms of phase transitions and the formation of possible structural defects thereof is the key to the synthesis of materials with desired and regulated properties. In this paper, we propose another mechanism for the H–T phase transitions in MoS<sub>2</sub> layer, which might be realized not only under electron doping, but under shock-wave propagation, too. Namely, the H–T transition is considered as an in-plane compression of a monolayer along *armchair* and/or *zigzag* directions via formation of an intermediate metastable “square” phase (S-phase) not yet disclosed on the minimum energy paths using DFT NEB method [26, 27, 29]. In addition, a relationship is established between the different scenarios of subsequent structure relaxations of S-phase into H-phase and the experimentally observed grain boundaries within the H-phase [30–35].

## 2. Computational details

As the basic models for the study of the H–T phase transition the supercells of both polymorphic single H- and T-layers of MoS<sub>2</sub> in rectangular  $a\sqrt{3} \times a = b \times a$  representation were employed, where  $a$  is the in-plane lattice parameter (Fig. 1). The atomic positions within supercells were optimized, while their lattice parameters were fixed and varied using the step 1% within 85%–150%  $a_0$  and 65%–120%  $b_0$ , where  $a_0$  and  $b_0$  are equilibrium lattice parameters.

All quantum-chemical calculations were performed within the framework of the density-functional theory (DFT) using the SIESTA 4.0 implementation [36]. The exchange-correlation potential was described within the Generalized Gradient Approximation (GGA) in the Perdew–Burke–Ernzerhof parametrization. The core electrons were treated within the frozen core approximation, applying norm-conserving Troullier–Martins pseudopotentials. The valence electrons were taken as  $4d^5 5s^1 5p^0$  for Mo and  $3s^2 3p^4 3d^0$  for S. The pseudopotential core radii were chosen as 2.43  $a_B$  for Mo4*d* and Mo5*s*, 2.62  $a_B$  for Mo5*p* states, and 1.69  $a_B$  for all S states, respectively. In all calculations, a double- $\zeta$  polarized basis set was used. The  $k$ -point mesh was generated by the method of Monkhorst and Pack. For  $k$ -point sampling, a cutoff of 15 Å was used. The real-space grid used for the numeric integrations was set to correspond to the energy cutoff of 300 Ry. The calculations of the pristine MoS<sub>2</sub> structures were performed using variable-cell and atomic position relaxations, with convergence criteria corresponding to the maximum residual stress of 0.1 GPa for each component of the stress tensor, and the maximum residual force component of 0.01 eV/Å.

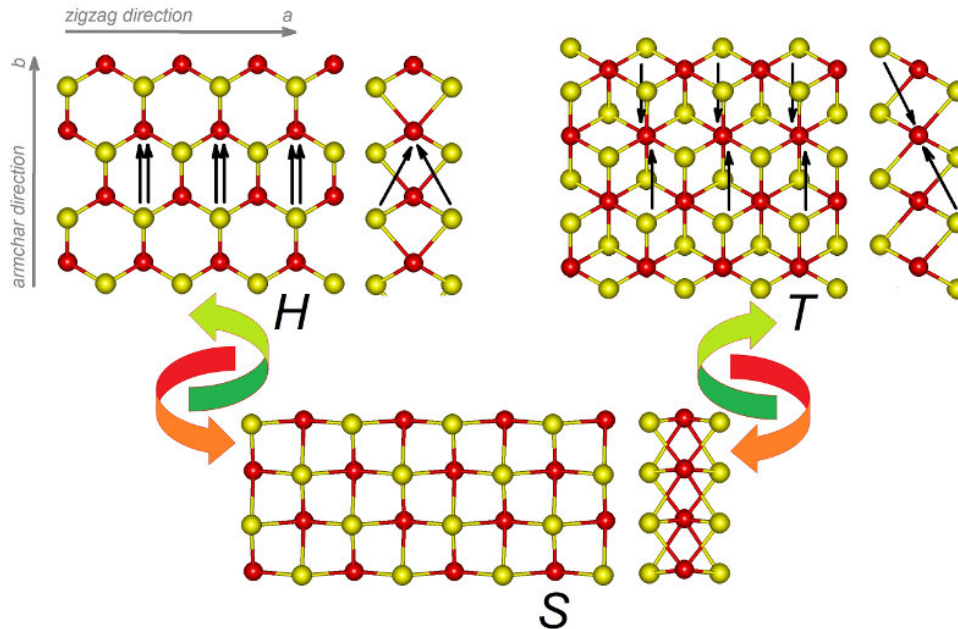


FIG. 1. Relation between H- and T-layers of MoS<sub>2</sub> established via in-plane compression along *armchair* direction of the layers suggests an existence of two-dimensional MoS<sub>2</sub> transition state with square lattice (S-phase). Ball-and-stick models represent the top and the side views on the structures with the DFT optimized geometries (Mo and S atoms are painted in red and yellow, respectively)

### 3. Results and Discussion

#### 3.1. S-phase of MoS<sub>2</sub>: a possible intermediate between H- and T-MoS<sub>2</sub>

Our main methodology for the study of H-T phase transition within individual MoS<sub>2</sub> monolayer involved the brute-force scan of the potential energy surface (PES) for both H- and T-phases depending on the imposed in-plane strain along two directions. Hence, a function of the potential energy can be simply mapped as a three-dimensional surface. Intuitively, the energy surfaces of both 2D polymorphs should share at least one joint point, when simply considering the deformation of 2D structures (Fig. 1). The in-plane compression of H-layer along *armchair* direction leads to rapprochement between a Mo atom and two S atoms opposing it as a couple within the same hexagonal ring. The similar compression of T-layer also leads to rapprochement between a Mo atom and two S atoms opposing it already as loners from two different hexagonal rings. One of the final common stages for both processes could be represented as a phase with regular square-like atom ordering – henceforth, S-phase. Apart of the lattice symmetry, the surmised intermediate S-phase should possess such coordination numbers of Mo and S atoms as 8 and 4, which are drastically different to the coordination in both known hexagonal phases. Therefore, we have preliminary examined by DFT calculations a possible stability and the properties of S-phase in comparison to those for the parent H- and T-MoS<sub>2</sub> layers.

The equilibrium lattice parameters  $a$  obtained in the present work for H- and T-layers are found equal 3.21 and 3.20 Å, respectively, which is in fair agreement with experimental and previous theoretical data [7, 37]. The geometry of the ideal S-MoS<sub>2</sub> with square lattice has not been reported before. It is found preserved after full optimization, yielding the lattice parameter  $a_0 = 2.99$  Å. The distances between sulfur planes within H-, T- and S-layers are equal to  $w_0 = 3.21, 3.27$  and  $2.98$  Å, respectively. Hence, while the surface area of unit cells remains roughly the same for all three polymorphs, a contraction of S-layer is observed in out-plane direction. The cubic MoS<sub>8</sub> polyhedra within S-layer are slightly distorted with distribution of Mo-S bond lengths  $l = 2.46\text{--}2.74$  Å, which fits at the lower bound  $l = 2.45$  and  $2.47$  Å within MoS<sub>6</sub> prisms and MoS<sub>6</sub> octahedra.

According to our calculations, T-MoS<sub>2</sub> is expectedly less stable, than H-MoS<sub>2</sub> on 0.85 eV/MoS<sub>2</sub>. The corresponding relative energy of S-MoS<sub>2</sub> was found to be close to this value and is 1.04 eV/MoS<sub>2</sub>. Since the stability difference between H- and T-MoS<sub>2</sub> is ruled mostly by electronic factor, T- and S-MoS<sub>2</sub> could share common features in electronic structure. The calculated electronic band structures for all three MoS<sub>2</sub> layers are drawn on Fig. 2. H-MoS<sub>2</sub> is semiconductor with the direct K–K band gap of 1.63 eV. The top edge of the valence band at  $-2 \dots -1$  eV relative the Fermi level as well as the bottom of conduction band are presented by Mo4*d*-states. The valence band below  $-2$  eV is mostly composed of S3*p*-states. In contrast, both T- and S-MoS<sub>2</sub> layers have a metal-like character. Like in the case of H-MoS<sub>2</sub> the valence band of occupied S3*p* states can be found below  $-3$  eV, while Mo4*d*-states form the bands hosting the Fermi level.

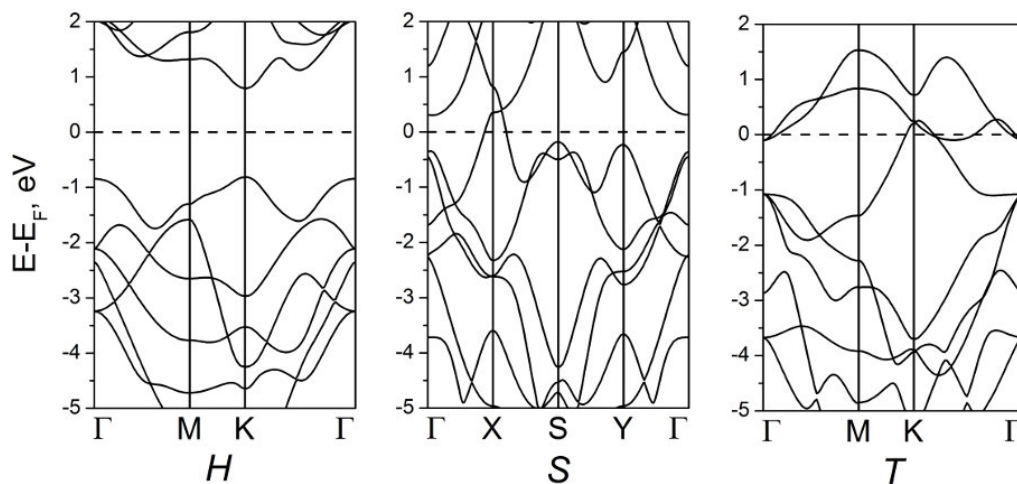


FIG. 2. Electronic band structures for H-, S- and T-layers of MoS<sub>2</sub>. DFT calculations

In terms of ligand field theory the semiconducting nature of H-MoS<sub>2</sub> is caused by the splitting of the Mo4*d* levels within trigonal prismatic field into the levels of the fully occupied Mo4*d*<sub>z<sup>2</sup></sub> orbital and the unoccupied Mo4*d*<sub>xy</sub>, Mo4*d*<sub>x<sup>2</sup>-y<sup>2</sup></sub>, Mo4*d*<sub>xz</sub> and Mo4*d*<sub>yz</sub> orbitals. Octahedral crystal field in T-MoS<sub>2</sub> splits the Mo4*d* levels into three

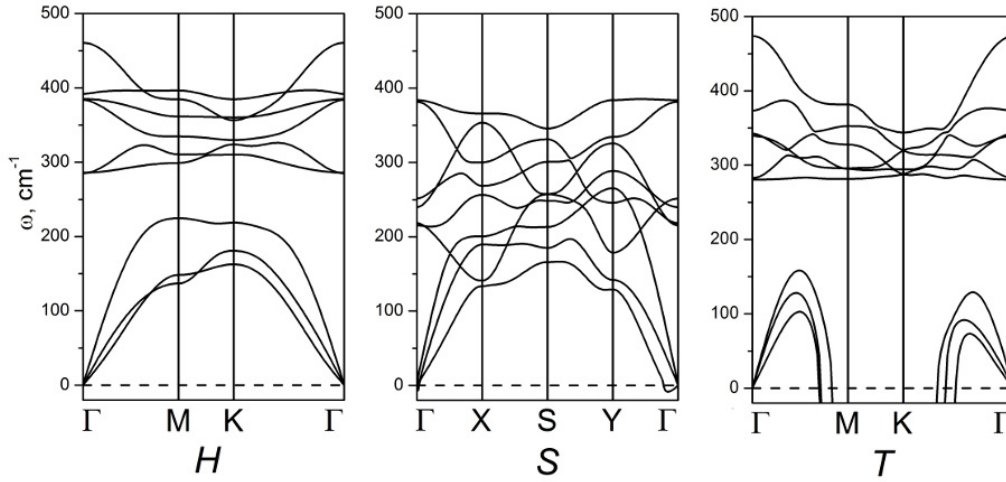


FIG. 3. Phonon band structures for H-, S- and T-layers of MoS<sub>2</sub>. DFT calculations

degenerate Mo4d<sub>xy,yz,xz</sub> levels occupied with only two electrons and the unoccupied Mo4d<sub>z<sup>2</sup></sub> and Mo4d<sub>x<sup>2</sup>-y<sup>2</sup></sub> levels. Such partial population is not beneficial, hence, stimulating the Jahn-Teller distortion of MoS<sub>6</sub> octahedron and the reconstruction of T-MoS<sub>2</sub> into a T'-MoS<sub>2</sub> phase. The splitting of the Mo4d levels in cubic field of S-MoS<sub>2</sub> is opposite to the former: every Mo4d<sub>z<sup>2</sup></sub> and Mo4d<sub>x<sup>2</sup>-y<sup>2</sup></sub> level is occupied by single electron, while Mo4d<sub>xy,yz,xz</sub> levels are unoccupied. Such electron configuration should be more resistant against the Jahn-Teller distortion, inhibiting a reconstruction and, possibly, prolonging the life-time of intermediate S-MoS<sub>2</sub> phase. To establish a dynamic stability of the intermediate the phonon band structures have been calculated for all three MoS<sub>2</sub> phases (Fig. 3). No imaginary frequency is obtained for the kinetically stable H-MoS<sub>2</sub>. In contrast, a part of the Brillouin zone in the band structure of T-MoS<sub>2</sub> contains a deep “pocket” of negative dispersion curves, which should be attributed to kinetic instability of the compound. The phonon band structure of S-MoS<sub>2</sub> is reminiscent of that for H-MoS<sub>2</sub>, yet, demonstrating the crossing of acoustic and optical modes. Here, a single phonon dispersion curve forms a small “pocket” of negative values at  $\Gamma$ -point. If not related to a numerical error of DFT calculation, it may refer to a long-living state.

### 3.2. Energy landscape of MoS<sub>2</sub> monolayer

The potential energy surfaces of H- and T-layers of MoS<sub>2</sub> have been calculated as the total energies relative to the total energy of H-layer at equilibrium. PES for T-layer lies mostly above PES of H-layer. Therefore, the former is mapped in the mirror  $a/a_0$  coordinates for a better perception (Fig. 4). PES of H-layer is characterized by single global minimum and a continuous up-hill energy valley along the decrease of  $b$  lattice parameter (i.e. upon shrinkage along *armchair* direction of the layer). The valley egresses a plateau of energies corresponding to S-MoS<sub>2</sub> layer. PES of T-layer unveils the presence of three minima in accordance to the three known monoclinic T'-phases of MoS<sub>2</sub> [21], arising from the reconstructions of hexagonal T-layer. Therefore, in addition to kinetic instability, the perfect environment of Mo atoms within T-layer is not the most thermodynamically stable one among octahedral coordinations.

The minimal energy paths plotted on the PES's of H- and T-layers (closed circles, Fig. 4) demonstrate that the global minima are separated by an energy barrier. Though, these paths are not strictly aligned along  $a/a_0$  coordinate and should be connected via the energy plateau of S-layer. The cross section of both PES's along these paths yields a classical picture of the transition between two states, requiring the passage of an energy barrier (Fig. 5). The energy barriers estimated using our brute-force scan of the MoS<sub>2</sub> energy map are equal to 1.66 eV for H→T transition, 0.83 eV and 1.06 eV for T→H and T'→H transitions, respectively, which are in-between the values found from the DFT-based NEB approach [29] and from the DFT analysis of consecutive transition states [26]. However, the energy path established here demonstrates the existence of a flattened part of the energy barrier, related to the S-MoS<sub>2</sub> phase as the transition state.

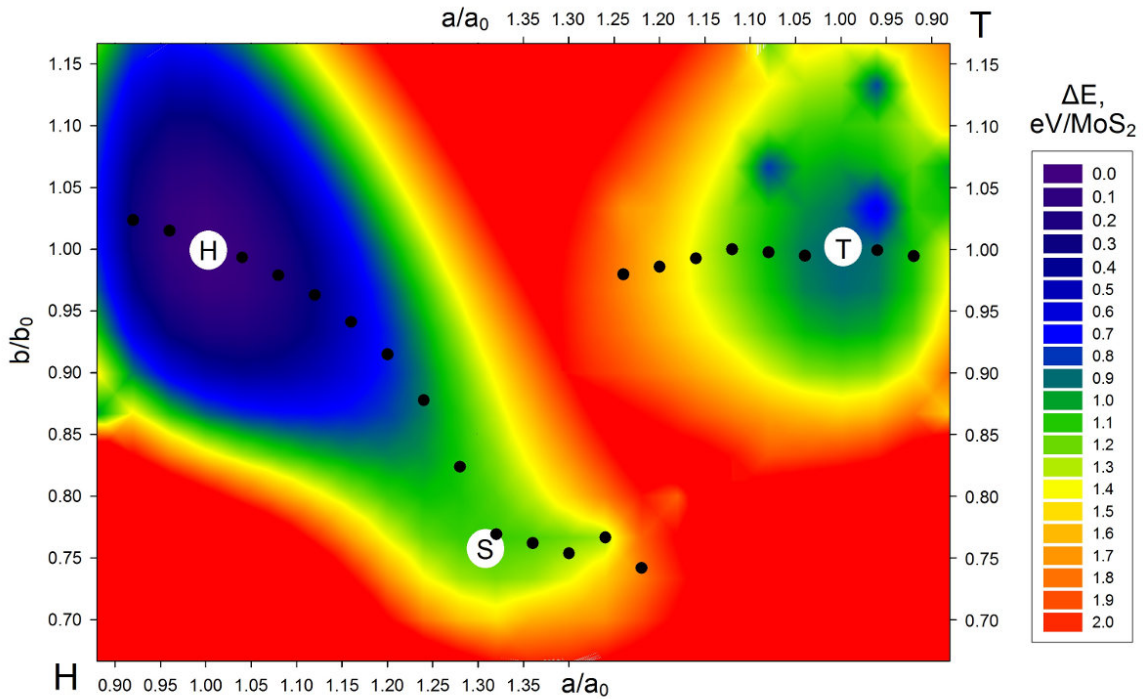


FIG. 4. Energy landscape depending on the lattice parameters for single MoS<sub>2</sub> layer unveils the equilibrium positions of H-, T- and S-phases (large open circles) and the minimal energy path between H and T phases (small closed circles). All energies  $\Delta E$  are given relative to the most stable H-MoS<sub>2</sub> phase. DFT calculations

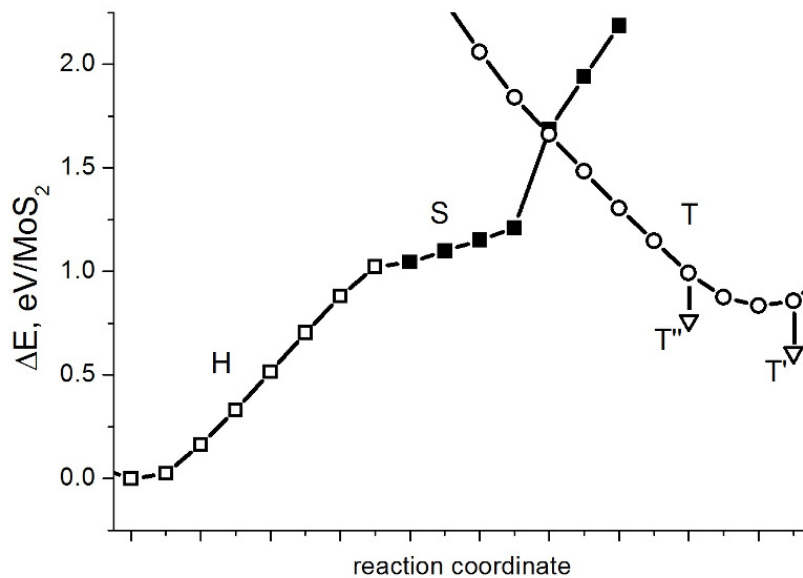


FIG. 5. Energy path during H $\leftrightarrow$ T transition within a MoS<sub>2</sub> monolayer as derived from energy maps for both H- and T-phases (Fig. 4).  $\Delta E$  values for hexagonal H- and T-phases are plotted using open squares and circles, for square S-phase using closed squares, for reconstructed monoclinic T'-, T''-phases using open triangles. DFT calculations

#### 4. Summary

The full energy mapping has disclosed a complicated energy landscape for MoS<sub>2</sub> layer, including the field of intermediate state of square lattice S-MoS<sub>2</sub> between hexagonal lattices of H- and T-MoS<sub>2</sub>. Hence, the phase transitions of MoS<sub>2</sub> between H- and T-phases or these in related MX<sub>2</sub> compounds may be not considered as a simple gliding of X planes within the molecular MX<sub>2</sub> layer. While the direct registration of S-MoS<sub>2</sub> remains an open problem, the traces of the manifestation of this state can be searched, analyzing the structural chemistry of two-dimensional MoS<sub>2</sub> booming in the recent years.

Several possible defect types have been visualized within the molecular layers of MoS<sub>2</sub> and related dichalcogenides: point vacancies within metal or chalcogen sublattices, point-like reconstructions and extended line defects, grain boundaries, doping or adsorbed atoms, which can affect the electronic, transport, optical properties of the compounds [38]. Much attention was paid to the grain boundaries and line defects. One of the scenarios of their origin is regarded to a merging of two growing nanoplates oriented relative to each other at a certain angle. According to [29], the grain boundary with the lowest formation energy in H-MoS<sub>2</sub> is the linear defect 4|4P consisting of four-membered cycles. A similar type of defect was observed at the junction of the H and T phases [30]. Other types of linear defects are also observed in the experiment, for example, squares and octagons or pentagons and heptagons among the hexagonal pattern of H-MoS<sub>2</sub> (4|8|4 and 5|7 defects) [31, 32].

However, the rise of these extended and perfectly organized grain boundaries in MoS<sub>2</sub> can also be related to the different tracks of relaxation of intermediate S-MoS<sub>2</sub> layer once appeared. A few examples are depicted on Fig. 6. The synchronous dissociation of cubic units MoS<sub>8</sub> within S-MoS<sub>2</sub> layer into distorted prisms MoS<sub>6</sub> gives a characteristic parquet-like pattern, which relaxes into perfect hexagonal H-MoS<sub>2</sub> layer (1, Fig. 6). The violations during such dissociation, e.g. due to a local mechanical strain or due to a substrate underneath, can finalize in various point-like or linear defects, including the grain boundaries observed in experiments [32, 33].

Therefore, irrespective the direct observation of intermediate S-MoS<sub>2</sub> layer, its model can serve as a useful tool for the construction of model defective MoS<sub>2</sub> layers.

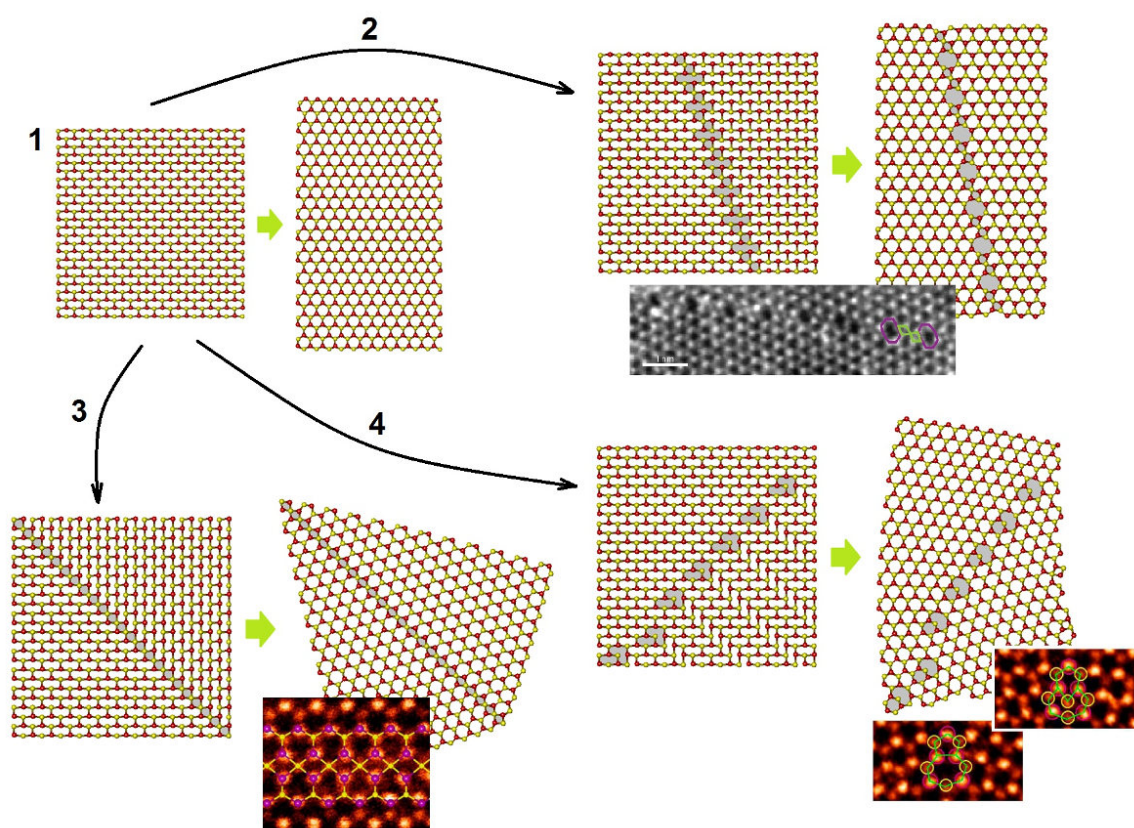


FIG. 6. The reconstruction tracks of S-MoS<sub>2</sub> layer can lead not only to the perfect H-MoS<sub>2</sub> layer (1), but to a wealth of line defects like these observed experimentally [32,33]: 4|4|8 grain boundary (2), 4|4 grain boundary (3), 6|8 and 5|7 grain boundaries (4) etc.

## Acknowledgment

The work was performed within the order from Ministry of Science and Higher Education of the Russian Federation (No. 0397-2019-0003).

## References

- [1] Chen Z., Liu X., Liu Y., Gunsell S., Luo J. Ultrathin MoS<sub>2</sub> Nanosheets with Superior Extreme Pressure Property as Boundary Lubricants. *Sci. Rep.*, 2015, **5**, P. 12869.
- [2] Radisavljevic B., Radenovic A., Brivio J., Giacometti V., Kis A. Single-layer MoS<sub>2</sub> transistors. *Nat. Nanotechnol.*, 2011, **6**, P. 147–150.
- [3] Desai S.B., Madhupathy S.R., Sachid A.B., Llinas J.P., Wang Q., Ahn G.H., Pitner G., Kim M.J., Bokor J., Hu C., Wong H.-S.P., Javey A. MoS<sub>2</sub> transistors with 1-nanometer gate lengths. *Science*, 2016, **354**(6308), P. 99–102.
- [4] Guan Z., Lian C.-S., Hu S., Ni S., Li J., Duan W. Tunable Structural, Electronic, and Optical Properties of Layered Two-Dimensional C<sub>2</sub>N and MoS<sub>2</sub> van der Waals Heterostructure as Photovoltaic Material. *J. Phys. Chem. C*, 2017, **121**(6), P. 3654–3660.
- [5] Yore A.E., Smithe K.K.H., Jha S., Ray K., Pop E., Newaz A.K.M. Large array fabrication of high performance monolayer MoS<sub>2</sub> photodetectors. *Appl. Phys. Lett.*, 2017, **111**, P. 043110.
- [6] Bergmann, H.; Czeska, B.; Haas, I.; Mohsin, B.; Wandner, K.-H. Gmelin Handbook of Inorganic and Organometallic Chemistry. *Springer-Verlag*, Berlin, 1992, Vol. B7.
- [7] He Z., Que W. Molybdenum disulfide nanomaterials: Structures, properties, synthesis and recent progress on hydrogen evolution reaction. *Appl. Mater. Today*, 2016, **3**, P. 23–56.
- [8] Cao Z.-Y., Hu J.-W., Goncharov A.F., Chen X.-J. Nontrivial metallic state of MoS<sub>2</sub>. *Phys. Rev. B*, 2018, **97**, P. 214519.
- [9] Zhuang Y., Dai L., Wu L., Li H., Hu H., Liu K., Yang L., Pu C. Pressure-induced permanent metallization with reversible structural transition in molybdenum disulfide. *Appl. Phys. Lett.*, 2017, **110**, P. 122103.
- [10] Liu Q., Li X., He Q., Khalil A., Liu D., Xiang T., Wu X., Song L. Gram-Scale Aqueous Synthesis of Stable Few-Layered 1T-MoS<sub>2</sub>: Applications for Visible-Light-Driven Photocatalytic Hydrogen Evolution. *Small*, 2015, **11**, P. 5556–5564.
- [11] Xie X., Kang J., Cao W., Chu J.H., Gong Y., Ajayan P.M., Banerjee K. Designing artificial 2D crystals with site and size controlled quantum dots. *Scientific Reports*, 2017, **7**, P. 9965.
- [12] Enyashin A.N., Seifert G. Density-functional study of Li<sub>x</sub>MoS<sub>2</sub> intercalates (0 ≤ x ≤ 1). *Comp. Theor. Chem.*, 2012, **999**, P. 13–20.
- [13] Enyashin A.N., Yadgarov L., Houben L., Popov I., Weidenbach M., Tenne R., Bar-Sadan M., Seifert G. New Route for Stabilization of 1T-WS<sub>2</sub> and MoS<sub>2</sub> Phases. *J. Phys. Chem. C*, 2011, **115**, P. 24586–24591.
- [14] Kim S., Song S., Park J., Yu H.S., Cho S., Kim D., Baik J., Choe D.-H., Chang K.J., Lee Y.H., Kim S.W., Yang H. Long-Range Lattice Engineering of MoTe<sub>2</sub> by 2D Electride. *Nano Lett.*, 2017, **17**(6), P. 3363–3368.
- [15] Kvashnin D.G., Chernozatonskii L.A. Electronic and Transport Properties of Heterophase Compounds Based on MoS<sub>2</sub>. *JETP LETTERS*, 2017, **105**(4), P. 250–254.
- [16] Acerce M., Voiry D., Chhowalla M. Metallic 1T phase MoS<sub>2</sub> nanosheets as supercapacitor electrode materials. *Nat. Nanotechnol.*, 2015, **10**, P. 313–318.
- [17] Jiang L., Zhang S., Kulich S.A., Song X., Zhu J., Wang X., Zeng H. Optimizing Hybridization of 1T and 2H Phases in MoS<sub>2</sub> Monolayers to Improve Capacitances of Supercapacitors. *Mater. Res. Lett.*, 2015, **3**, P. 177–183.
- [18] Cheng P., Sun K., Hu Y.H. Memristive Behavior and Ideal Memristor of 1T Phase MoS<sub>2</sub> Nanosheets. *Nano Lett.*, 2016, **16**(1), P. 572–576.
- [19] Cheng P., Sun K., Hu Y.H. Mechanically-induced Reverse Phase Transformation of MoS<sub>2</sub> from Stable 2H to Metastable 1T and Its Memristive Behavior. *RSC Adv.*, 2016, **6**, P. 65691–65697.
- [20] Sun T., Zhang H., Wang X., Liu J., Xiao C., Nanayakkara S.U., Blackburn J.L., Mirkin M.V., Miller E.M. Nanoscale mapping of hydrogen evolution on metallic and semiconducting MoS<sub>2</sub> nanosheets. *Nanoscale Horiz.*, 2019.
- [21] Heising J., Kanatzidis M.G. Structure of Restacked MoS<sub>2</sub> and WS<sub>2</sub> Elucidated by Electron Crystallography. *J. Am. Chem. Soc.*, 1999, **121**, P. 638–643.
- [22] Zhuang H.L., Johannes M.D., Singh A.K., Hennig R.G. Doping-controlled phase transitions in single-layer MoS<sub>2</sub>. *Phys. Rev. B*, 2017, **96**, P. 165305.
- [23] Wang Z.F., Jin K.-H., Liu F. Computational design of two-dimensional topological materials. *WIREs Comput. Mol. Sci.*, 2017, **7**, P. e1304.
- [24] Eda G., Fujita T., Yamaguchi H., Voiry D., Chen M., Chhowalla M. Coherent Atomic and Electronic Heterostructures of Single-Layer MoS<sub>2</sub>. *ACS Nano*, 2012, **6**, P. 7311–7317.
- [25] Eda G., Yamaguchi H., Voiry D., Fujita T., Chen M., Chhowalla M. Photoluminescence from Chemically Exfoliated MoS<sub>2</sub>. *Nano Lett.*, 2011, **11**, P. 5111–5116.
- [26] Ryzhikov M.R., Slepikov V.A., Kozlova S.G., Gabuda S.P., Fedorov V.E. Solid-State Reaction as a Mechanism of 1T↔2H Transformation in MoS<sub>2</sub> Monolayers. *J. Comput. Chem.*, 2015, **36**, P. 2131–2134.
- [27] Gao G., Jiao Y., Ma F., Jiao Y., Waclawik E., Du A. Charge Mediated Semiconducting-to-Metallic Phase Transition in Molybdenum Disulfide Monolayer and Hydrogen Evolution Reaction in New 1T' Phase. *J. Phys. Chem. C*, 2015, **119**(23), P. 13124–13128.
- [28] Lin Y.-C., Dumcenco D.O., Huang Y.-S., Suenaga K. Atomic mechanism of the semiconducting-to-metallic phase transition in single-layered MoS<sub>2</sub>. *Nat. Nanotechnol.*, 2014, **9**, P. 391–396.
- [29] Guo Y., Sun D., Ouyang B., Raja A., Song J., Heinz T.F., Brus L.E. Probing the Dynamics of the Metallic-to-Semiconducting Structural Phase Transformation in MoS<sub>2</sub> Crystals. *Nano Lett.*, 2015, **15**, P. 5081–5088.
- [30] Komsa H.-P., Krashennnikov A.V. Engineering the Electronic Properties of Two-Dimensional Transition Metal Dichalcogenides by Introducing Mirror Twin Boundaries. *Adv. Electron. Mater.*, 2017, **3**, P. 1600468.
- [31] Lin Y.-C., Yeh C.-H., Lin H.-C., Siao M.-D., Liu Z., Nakajima H., Okazaki T., Chou M.-Y., Suenaga K., Chiu P.-W. Stable 1T WS<sub>2</sub> monolayer and its junctions: growth and atomic structures. *ACS Nano*, 2019, **12**, P. 12080–12088.
- [32] Najmaei S., Liu Z., Zhou W., Zou X., Shi G., Lei S., Yakobson B.I., Idrobo J.-C., Ajayan P.M., Lou J. Vapour phase growth and grain boundary structure of molybdenum disulfide atomic layers. *Nat. Mater.*, 2013, **12**, P. 754.

- [33] van der Zande A.M., Huang P.Y., Chenet D.A., Berkelbach T.C., You Y., Lee G.-H., Heinz T.F., Reichman D.R., Muller D.A., Hone J.C. Grains and grain boundaries in highly crystalline monolayer molybdenum disulphide. *Nat. Mater.*, 2013, **12**, P. 554–561.
- [34] Ghorbani-Asl M., Enyashin A.N., Kuc A., Seifert G., Heine T. Defect-induced conductivity anisotropy in MoS<sub>2</sub> monolayers. *Phys. Rev. B*, 2013, **88**, P. 245440.
- [35] Taha D., Mkhonta S.K., Elder K.R., Huang Z.-F. Grain Boundary Structures and Collective Dynamics of Inversion Domains in Binary Two-Dimensional Materials. *Phys. Rev. Lett.*, 2017, **118**, P. 255501.
- [36] Soler J.M., Artacho E., Gale J.D., Garcia A., Junquera J., Ordejon P., Sanchez-Portal D. The SIESTA method for *ab initio* order-*N* materials simulation. *J. Phys. Condensed Matter*, 2002, **14**, P. 2745–2779.
- [37] Kan M., Wang J.Y., Li X.W., Zhang S.H., Li Y.W., Kawazoe Y., Sun Q., Jena P. Structures and Phase Transition of a MoS<sub>2</sub> Monolayer. *J. Phys. Chem. C*, 2014, **118**, P. 1515–1522.
- [38] Enyashin A.N., Seifert G. Electronic properties of MoS<sub>2</sub> monolayer and related structures. *Nanosystems: physics, chemistry, mathematics*, 2014, **5**, P. 517–539.